Mon. Not. R. astr. Soc. (1981) **195**, 787–804

High resolution line profiles in the Seyfert galaxy NGC 3783: The structure of the emitting regions

Didier Pelat★, Danielle Alloin★ and Robert A. E. Fosbury† *European Southern Observatory, c/o CERN, 1211 Geneva 23, Switzerland*

Received 1980 October 7; in original form 1980 April 9

Summary. We present the analysis of emission line profiles in the Seyfert nucleus of NGC 3783. The lines, covering a wide range of ionization from O^0 up to Fe^{9+}, are analysed from IPCS or electronographic data obtained with resolutions from 0.03 to 0.12 nm. When the signal-to-noise ratio allowed it, a precise analysis generally showed a broad, blueshifted component in the line under consideration. The main results of this study are the following:

(1) There appears to be a relationship between the FWHI of the main component within a line and the ionization potential of the corresponding ion.

(2) For all the forbidden lines, there is a relationship between the FWHI of any component and its emission shift, with broad components and high ionization species being more blueshifted: for example, the main broad component in the [Fe X] line is blueshifted by 400 km s^{-1} with respect to the [O I], [O II] and [N II] emission velocity.

(3) The Balmer lines show components corresponding to these forbidden line regions but their main contribution is from a very broad (3000 km s^{-1}) redshifted (+200 km s^{-1}) component. The results are most plausibly interpreted in the framework of a central massive object surrounded by an accretion disc (AD), for which we derive an inclination of 15° and a mean radius of $10^3 R_S$. Arguments are then presented that only the high-density region ($N_e > 10^{10}$ cm^{-3}) is concerned with the AD itself, while the forbidden-line region is dominated by a radial rather than a rotational velocity field whose magnitude increases towards the centre where the photo-ionizing source lies. Consideration of the ionization equilibrium together with the observed radial velocities, assumed to be from infalling matter, favour the picture of filaments clustering towards the centre and decelerated by frictional mechanisms which also increase the turbulence of the medium.

★On leave of absence from Meudon Observatory.
† Present address: Royal Greenwich Observatory, Herstmonceux Castle, Hailsham, East Sussex, BN27 1RP.

1 Introduction

Following previous work on NGC 1068 and 4151, we continue our analysis of emission line profiles in Seyfert nuclei to elucidate the structure of the emitting regions and to derive observational constraints on theoretical models.

To date, only moderate dispersion results have been published, apart from a few studies of NGC 1068 and 4151 (Walker 1968a, b; Ulrich 1973; Glaspey *et al.* 1976a, b; Pelat & Alloin 1980, 1981) which were devoted to emission line profiles. Besides that, interest has been devoted mainly to the permitted lines, because of their extremely broad profiles in Seyfert 1 objects and their link with the puzzling innermost dense regions of the nucleus, commonly called broad line region (BLR). However, it seems quite evident that any detailed analysis of the Balmer line profiles requires a knowledge of the forbidden narrower line region (NLR) since this region also contributes, although in a way varying from one object to the other, to the observed Balmer lines and thus contaminates the net Balmer line profile originating in the BLR. It is the pure broad line profiles which we need to compare with theoretical predictions from various models of the central object, and new results clearly demonstrate that the forbidden line region is not as homogeneous as was once thought.

The recent detailed analysis of the [O III] 500.68 and 495.89 nm lines in NGC 1068 and 4151 (Pelat & Alloin 1980, 1981) enables us to get a clearer picture of the forbidden line region: besides the cloudy structure (the clouds are seen individually) which lies in a region up to 10^2 pc from the centre, there exists an intermediate zone ($N_e \sim 10^5$ to 10^7 cm^{-3}) emitting a broad (1 to 1.5×10^3 km s^{-1}) component, blueshifted by up to a few hundred km s^{-1} with respect to the systemic velocity of the galaxy and responsible for up to half of the total [O III] flux. Other systematic wavelength shifts have been reported by Wilson (1979) for the [Fe X] 637.45 nm line in several Seyfert 1 nuclei (blueshift of about 3×10^2 km s^{-1} with respect to lower excitation emission lines) and by Grandi (1978) for the [Fe XI] 789.19 nm line (blueshift of up to 5×10^2 km s^{-1} with respect to a mean of lower excitation emission lines). Although IZw 1 is probably not a typical Seyfert 1, Phillips (1976) has noted that in that galaxy the high excitation forbidden lines [O III] and [Ne III] are broader than and blueshifted with respect to the lower excitation lines. Koski (1978) briefly reviews some other examples of wavelength shifts between high and low excitation lines (PKS 1510–08, IZw 1, 5C 3.100, Mk 268, PKS 1345 + 12). Moreover, in quasars the [Ne V] 342.58 nm line is usually found to be broader than the [O III] 500.68 nm line.

The following points emerge:

(i) There exists a distribution in linewidth among the forbidden lines, probably linked to a distribution of macroscopic kinematic energy within the different emitting zones.

(ii) Blueshifts are found for high excitation forbidden lines, with respect to the systemic velocity of the galaxy or to lower excitation lines.

It is interesting therefore to check these preliminary results by a careful investigation in a single object, making a quantitative analysis for each line of all the contributing zones. The observed profiles should be regarded as a composite, so that the decomposition of a set of forbidden lines within a particular Seyfert nucleus becomes a powerful probe of the structure and physical conditions in the emitting regions around the true nucleus.

In the present study, we have focused our attention on the forbidden line region in NGC 3783, a Seyfert 1 galaxy which is known to be a powerful X-ray emitter (Cooke *et al.* 1976; Elvis *et al.* 1978). A recent study by Ward (1978) shows that the forbidden lines emitted by NGC 3783 cover a large linewidth range (from 2×10^2 up to 8×10^2 km s^{-1}, FWHI), the lines being broader for higher ionization potentials. After presenting high-resolution observational data in Section 2, we discuss the method of analysis and provide

the results of the decomposition in Section 3. Section 4 is devoted to a discussion of the results and their relevance to the study of the intimate environment of Seyfert nuclei, while the main results of the study are summarized in Section 5.

2 Observational data

We obtained data with the Image Photon Counting System (IPCS) on the intermediate dispersion spectrograph at the Cassegrain focus of the 3.9-m Anglo-Australian telescope. Relevant information for these observations is provided in Table 1. Also, we used echelle-mode spectrograms obtained with the Echelle spectrograph (Baranne & Duchesne 1976) attached to the coudé focus of the 1.5-m telescope at La Silla observatory (European Southern Observatory). The detector was an electronic Lallemand–Duchesne camera loaded with Industrex Kodak plates. All relevant information for this observational material is summarized in Table 2. We did not use any field rotator because of the point-source aspect of the nucleus (< 2 arcsec). The spectroelectronographic data has been reduced at the Centre de Dépouillement des Clichés Astronomiques (INAG), following the procedure already described by Pelat & Alloin (1980a). The resultant profiles of the [O III] 500.68 nm line obtained with each of these instruments are presented in Fig. 1.

Instrumental baselines were removed using observations of standard stars. The nominal resolution quoted in Tables 1 and 2 corresponds to the measured FWHI of the comparison lines which, to a good approximation, are Gaussian in both sets of data.

Table 1. Observational IPCS data.

Analysed line λ_0 (nm)	Dispersion (nm mm^{-1})	Nominal resolution (nm)	Slit width★ (arcsec)	Date
Hβ 486.13 [O III] 495.89, 500.68	1.0	0.05	0.4	1977 January 1
[O II] 372.62, 372.89 [Fe VII] 376.03 [Ne III] 386.87	3.0	0.12	1.2	1977 July 20
[Ne V] 342.58	3.0	0.12	1.1	1977 July 22
[Fe VII] 608.69 [O I] 630.02, 636.39 [Fe X] 637.45 Hα 656.28 [N II] 654.81 658.34	2.5	0.12	1.4	1976 December 13

★The slit was always oriented along the east–west direction. we have verified that the atmospheric differential refraction was negligible with respect to the slit width, in the wavelength interval considered within each spectrum.

Table 2. Observational electronographic data.

Analysed line λ_0 (nm)	Dispersion (nm mm^{-1})	Nominal resolution (nm)	Exposure time (h)	PA at mid-exposure (deg)	Slit width (μm; arcsec)	Date
[O III] 500.68	1.051	0.03	3.75	182	600; 2.8	1977 February 16
[O III] 500.68	0.919	0.03	3.3	185	600; 2.8	1977 February 17

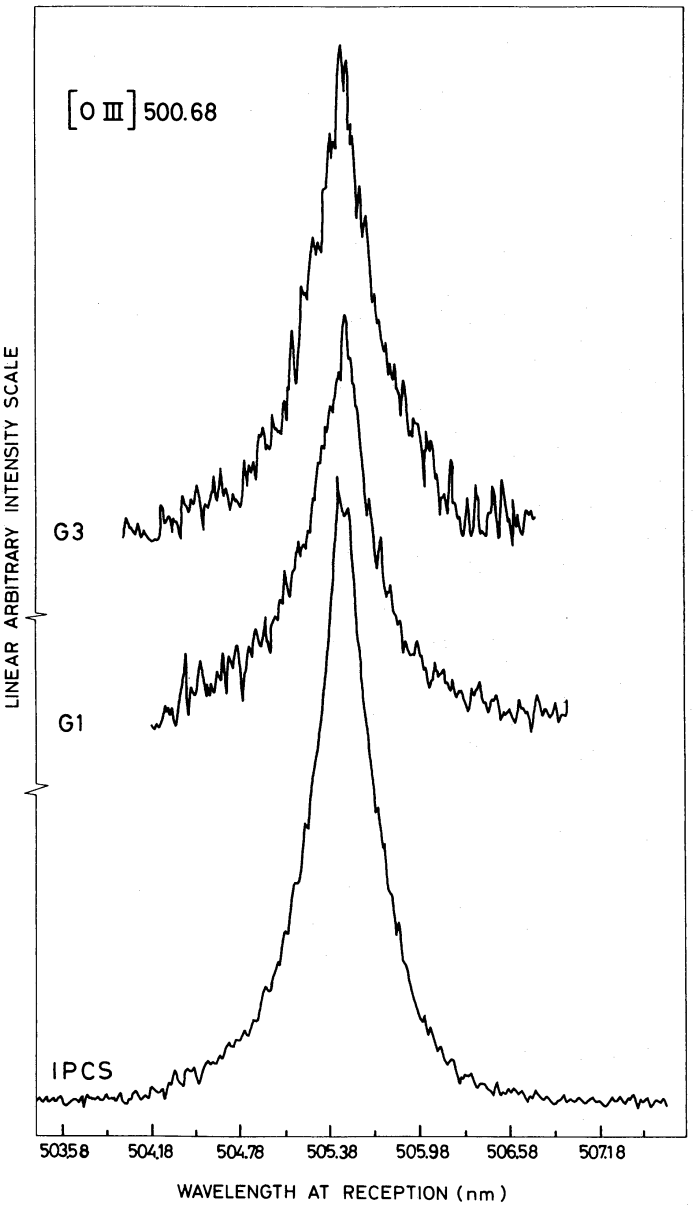

Figure 1. Intensity tracings for three independent [O III] 500.68 nm line profiles. The upper ones are from electronographic data, while the lower one refers to IPCS data.

3 Analysis of the data and results

Taking advantage of the increased spectral resolution, at least for the [O III] 500.68 nm and Hβ 486.13 nm lines, by a factor of around 10 compared to the most recent available data, we were able to separate these data into different contributing components. For this purpose we used a program already described by Pelat & Alloin (1980), based upon least squares fitting techniques (Fletcher & Powell 1963; James 1972). It is clear, even by visual inspection, that the line profiles are not symmetrical. The entire line cannot be represented by a single simple function of a Gaussian, Lorentzian or Voigt shape, In order to model this behaviour, we have chosen to decompose the profile into several Gaussian components whose FWHI, intensity and position are free or constrained parameters, depending on the amount of *a priori* physical information we have. Assuming a Gaussian profile implies that

random turbulent motion within the gas is the main source of line broadening. This assumption appears to be the simplest one to use in the absence of any clear and strong astrophysical reason for selecting, instead, a Lorentz or Voigt profile, the latter having the disadvantage of containing another free parameter.

We wish to stress the limitations of such a mathematical treatment: the solution is not unique given initial data of limited signal-to-noise ratio. The solution provided in each case corresponds to the local minimum of the quadratic error near the initial guess. The stability of the solutions was investigated by trying a variety of initial guesses, some quite far from the final solution.

The continuum is automatically chosen by the program according to a preselected formula (a constant, a polynomial fit of a given degree, etc.).

A few comments should be given first:

(i) The simplest way of interpreting such an analysis of a complex line profile is to attribute each component to a different region of emitting material. However, this approach can be wrong if any large-scale organized motion takes place in the emitting regions (e.g. Keplerian rotation around a massive central body). Moreover, the number of components into which we are able to analyse a particular line depends on the signal-to-noise ratio and on the resolution of the data, quantities which vary from one line to the other. In one such case lines which should give similar results, [Ne III] 386.87 nm and [O III] 500.68 nm, were in fact respectively analysed into two and three components. The parameters, FWHI and emission velocity, follow the same relationship between each other (see Section 4); but one finds the parameters that are relevant for the two zones of [Ne III] are intermediate between those for the three zones of [O III].

(ii) For all components appearing in the decomposition, with a FWHI less than 10 times the nominal resolution given in Table 3, we have applied a quadratic correction to account for instrumental broadening.

(iii) The resolution achieved in the positioning of a line is better than the nominal resolution. This is particularly true for the narrower components, and it is not surprising since, in our procedure, we use information over the whole of the line profile. On the other hand, velocities measured with respect to the comparison lines might suffer, in a few cases, from a slight systematic error due to the different illumination of the spectrograph collimator.

We present here the results obtained for the different lines particularly the emission wavelength shift of the different components, which we find to be correlated with their width.

3.1 FORBIDDEN LINE PROFILES

[O III] 500.68 nm: the analysis was conducted independently on the three available profiles. The minimum number of components to give a satisfactory fit is three. Decomposition for the IPCS data is displayed in Fig. 2. The three independent profiles give solutions in fairly good agreement (Table 3).

[O II] doublet 372.62, 372.89 nm: this was analysed using a single Gaussian component for each line and without specifying any constraint on the parameters: the best fit yields a separation of 0.29 nm (theoretical one: 0.275 nm) between the two lines, and a FWHI of 0.266 and 0.268 nm. This illustrates the degree of precision achieved in the analysis. Although it was not possible to represent each [O II] line of the doublet by more than one Gaussian component, we can state that the [O II] lines are free from any component broader than 0.5 nm, containing a significant fraction of the radiation. The profile is clearly different from that of the [O III] line.

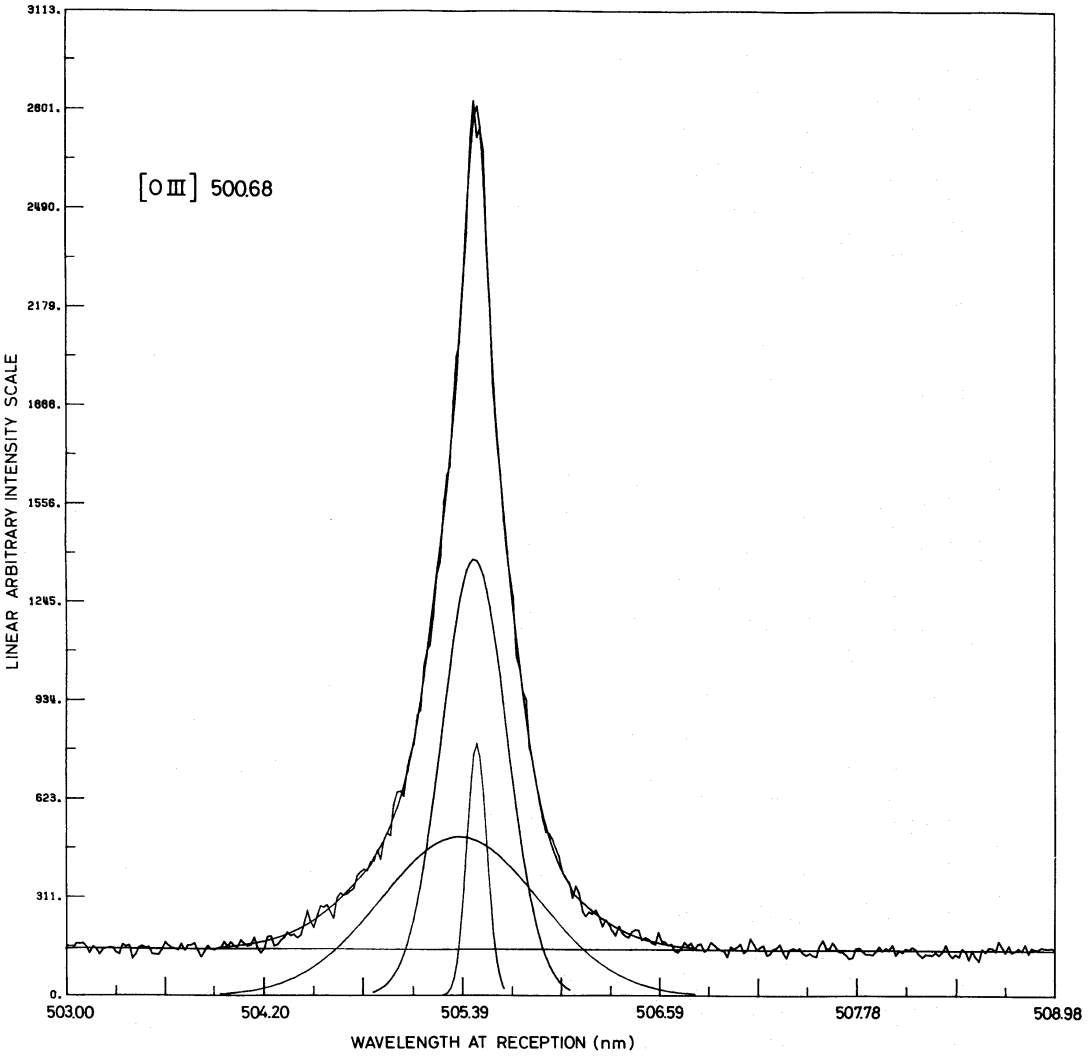

Figure 2. Gaussian decomposition of the [O III] 500.68 nm line.

[*Ne V*] *342.58 nm*: this is fitted best with a two-component analysis in order to account for the simultaneous presence of a narrow core and broad wings not centred on the peak.

[*Fe VII*] *376.03 and 608.69 nm*: these lines are each fitted by one component only, although some narrower feature might be present.

[*Ne III*] *386.87 nm*: although there are problems caused by blending with broad He and H lines, definitely requires a two-component analysis.

[*O I*] *630.02, 636.39 nm and* [*Fe X*] *637.45 nm*: these regions were more difficult to analyse. Aside from these lines, some other features are found in the decomposition which can be tentatively identified with [S III] 631.02 nm and He II 640.65 at a low intensity level. The [S III] line shows a FWHI and a blue velocity shift too large for its ionization potential (see section 4.2), and we suppose that some broad and blueshifted component of the [O I] 630.02 nm line is present. Bearing in mind the large critical density of [O I] lines, this would not be surprising.

We have imposed on the [O I] doublet the same FWHI, an intensity ratio of 3:1, and the known wavelength separation. For the [Fe X] line we find a broad component contributing

Table 3. Results of the analysis for forbidden lines.

Line, λ_0 [5] (nm)	Observed λ_r (nm)	Observed FWHI (nm)	V_{em} [1] heliocentric velocity (km s^{-1})	Nominal resolution (km s^{-1})	v_T [2] (km s^{-1})	E/E$_{tot}$ (%)	Notes	f_λ [6] (10^{-13} erg cm^{-2} s^{-1})
	505.38	1.12	2830		400	43	AAT, IPCS	4.17
[OIII] 500.68	505.47	0.46	2885	±15	165	48	1 nm mm^{-1}	4.66
	505.48	0.14	2890		50	9		0.87
	505.37	1.19	2820		420	60	Echelle	5.82
[OIII] 500.68	505.46	0.42	2875	±10	150	35		3.40
	505.49	0.13	2895		45	5		0.49
	505.41	0.95	2845		340	32	Echelle	3.10
[OIII] 500.68	505.50	0.49	2895	±10	175	58		5.63
	505.51	0.14	2900		50	10		0.97
[NeV] 342.58	345.91	0.65	2890	±35	330	90	AAT, IPCS	
	345.96	0.07	2930		30	10	3 nm mm^{-1}	
[OII] 372.62	376.25	0.24	2900	±35	120		AAT, IPCS	
372.89	376.54	0.24	2910		120		3 nm mm^{-1}	
[FeVII] 376.03 [3]	379.40	0.98	2660	±35	460		AAT, IPCS	
							3 nm mm^{-1}	
[NeIII] 386.87	390.57	0.94	2845	±35	430	66	AAT, IPCS	
	390.66	0.23	2910		100	34	3 nm mm^{-1}	
[FeVII] 608.69 [3]	613.90	1.37	2590	±35	400		AAT, IPCS	
							2.5 nm mm^{-1}	
[OI] 630.02	636.13	0.37	2930	±35	100	Imposed	AAT, IPCS	
639.39	642.62	0.37	2960		100	ratio 3:1	2.5 nm mm^{-1}	
[FeX] 637.45 [4]	642.77	3.87	2530		1080	71	AAT, IPCS	
	642.98	0.85	2620	±35	240	21	2.5 nm mm^{-1}	
	643.69	0.22	2960		60	8		
[NII] 654.81	661.05	0.33	2880	±35	90	Imposed	AAT, IPCS	
658.34	664.62	0.33	2880		90	ratio 1:3	2.5 nm mm^{-1}	

1. $V = (\lambda - \lambda_0/\lambda)c$. Relativistic effects in the case of NGC 3783 are negligible ($cz - V_t = 15$ km s^{-1}). c = 299792.9 km s^{-1}.
2. v_T = FWHI/1.67.
3. λ_0 from Nussbaumer & Osterbrock (1970). [Fe VII] 608.69 is assumed to be free from any [Ca V] 608.59 contribution.
4. λ_0 from Rozelot (1970).
5. λ_0 for the other lines is from Bowen (1960).
6. Absolute fluxes after Osmer, Smith & Weedman (1974) obtained with an entrance circular diaphragm 10 arcsec in ϕ, 1972 December and 1973 January. They have not been corrected for reddening.

most of the energy in the line, and two other marginal components which, in the absence of any other plausible emission lines in that range, could represent other [Fe X] contributing zones. Of particular interest is the narrow [Fe X] component which we find to be emitted at about the same redshift as the [O I] lines and which might be associated with the narrow [Ne V] component since they show about the same emission velocity and the same width. Although the present solution is a preliminary one, this narrow component might be the signature of a diluted coronal gas where iron is collisionally ionized to the Fe^{9+} stage. The existence of such a region is still debated (Oke & Sargent 1968) and its importance, on theoretical grounds, certainly deserves better high-resolution observations in this wavelength range.

The [N II] 654.81 and 658.34 nm lines superimposed on Hα were constrained to have the same FHWI, an intensity ratio of 3:1, and a fixed wavelength separation.

3.2 ABSORPTION LINES

Several absorption features are present in the spectrum of NGC 3783. A narrow line, at λ 393.44 nm with a FWHI of 0.16 nm, has been attributed to a galactic Ca II 393.37 nm component at a heliocentric velocity of 35 km s^{-1}. A second absorption line is seen at λ 396.89 nm with a slightly larger FWHI (0.21 nm): it probably represents a blend of the corresponding galactic Ca II 396.85 nm component with some Ca II *K* line intrinsic to NGC 3783. The inferred velocities are compatible with the 35 km s^{-1} galactic feature and the mean velocity of NGC 3783, but do not enable us to improve the accuracy of either.

From two other IPCS spectra obtained at lower dispersion (13 nm mm^{-1}), not referred to in Table 1, absorption lines of the Na I 588.99 and 589.59 nm are detected in the blue wing of He I at a position compatible with the galactic *K* and *H* features discussed earlier.

3.3 PERMITTED LINE PROFILES

We have studied both the Hβ and Hα lines. The Hβ profile was analysed without any constraint on the parameters and led to the solution presented in Table 4 and shown in Fig. 3. We have verified that the Fe II multiplet 42 lines are too weak in NGC 3783 to contaminate the Hβ profile around 492.4 nm. The Hα profile was constrained to contain at least the two narrower components which had been found in the Hβ analysis, which correspond to nos 1 and 2 in the [O III] 500.68 nm profile. Results for the best Hα fit are given in Table 4 and the decomposition is presented in Fig. 4.

The narrower feature, no. 1, in the decomposition of both Hα and Hβ comes from a region represented by a mean turbulent velocity (v_T = FWHI/1.67) of around 100 km s^{-1}; whilst in the analysis of the [O III] 500.68 nm, given the better signal-to-noise ratio in this line, we were able to separate this into two components with v_T values of 50 and 165 km s^{-1}. For the remainder of the Hα and Hβ line profiles, a two-component decomposition, nos 3 and 4, provides a satisfactory fit.

One component, no. 3, is blueshifted with respect to the narrow core and contains around 13 and 16 per cent of the total Hβ and Hα fluxes respectively. From its turbulent velocity, $v_T \sim 700$ km s^{-1}, and its heliocentric velocity, 2470 km s^{-1}, it can be associated with the broad, blueshifted [Fe X = 637.45 nm component ($v_T \sim 1100$ km s^{-1}; heliocentric velocity 2530 km s^{-1}).

Table 4. Results of the analysis for Balmer lines.

Line, λ_0 (nm)	Observed λ_r (nm)	Observed FWHI (nm)	V_{em} helio-centric velocity (km s^{-1})	Nominal resolution (km s^{-1})	v_T (km s^{-1})	E/E_{tot} (per cent)	No. of compo-nent	f_λ (10^{-13} erg cm^{-2} s^{-1})
Hβ	490.062	1.78	2445		650	13	3	1.00
486.133	490.640	1.11	2805	±15	405	10	2	0.77
	490.798	0.28	2900		100	3	1	0.23
	491.265	4.70	3190		1715	74	4	5.70
Hα	661.671	2.59	2485		700	16	3	4.16
656.282	662.262	1.29	2755	±35	350	6	2	1.56
	662.525	0.33	2875		90	2.5	1	0.65
	663.162	6.39	3165		1730	75.5	4	19.63

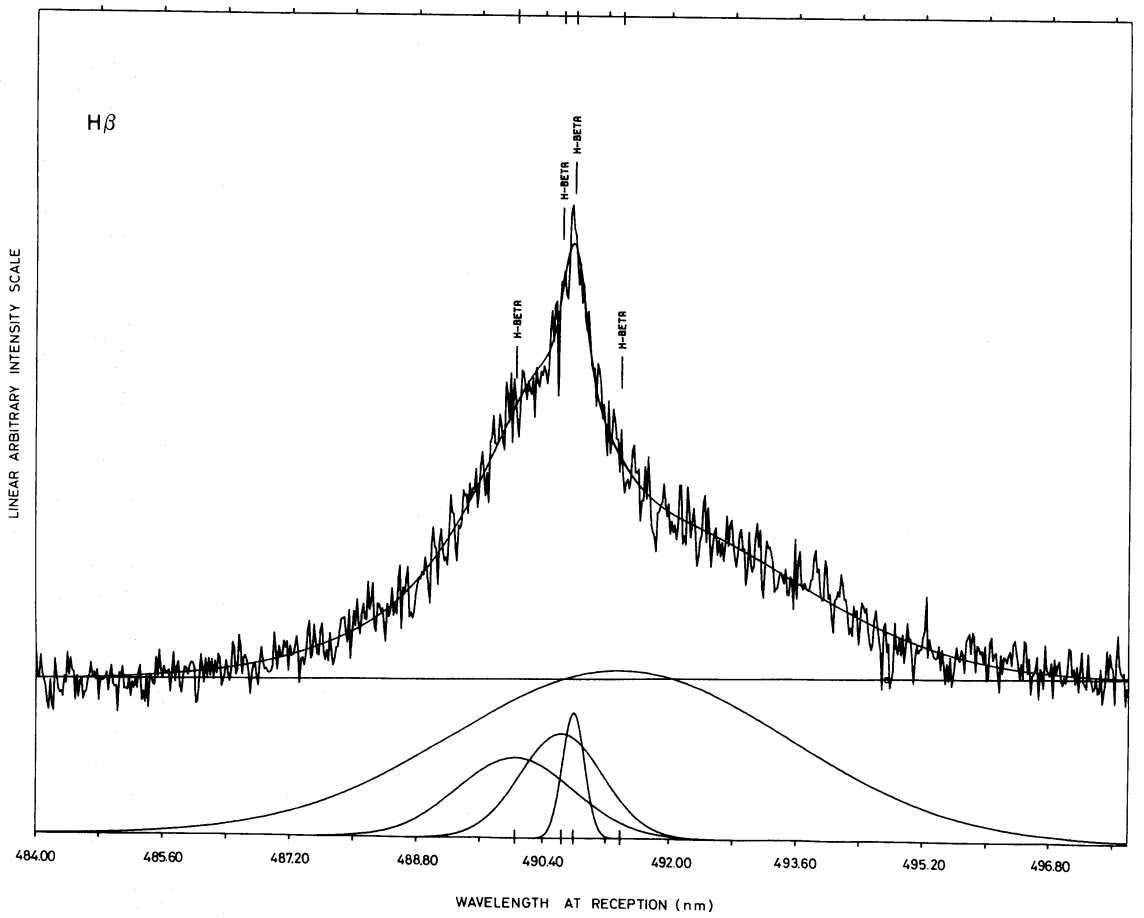

Figure 3. Gaussian analysis of the Hβ 486.13 nm line.

The main component, no. 4 (74 and 75.5 per cent of the Hβ and Hα fluxes, respectively), is found to be redshifted with a heliocentric velocity around 3180 km s^{-1} and a turbulent velocity $v_T \sim 1700$ km s^{-1}. This component, without any forbidden line counterpart, must be attributed to the high density region with $N_e \geqslant 10^{10}$ cm^{-3}. It is probably not well represented by a Gaussian profile owing to self-absorption effects (Netzer 1975; Ferland, Netzer & Shields 1979) and to possible kinematic effects due to a rapid rotation of the emitting matter (Gerbal & Pelat 1981). Consequently the large difference in wavelength shift which appears between components no. 4 and no. 3 could be slightly overestimated. The overall decomposition is satisfactory, however, in the sense that it allows the identification of the different emitting zones from which forbidden lines also originate, up to the electron density at which [Fe x] 637.45 is collisionally de-excited, i.e. 10^{10} cm^{-3}. These components, nos 1, 2 and 3, correspond well with components found in different forbidden lines, The blue or red shoulders commonly quoted in the literature for the Balmer line profiles might be explained by the relative strengths of the blue component no. 3 and the red one no. 4.

Besides this, we recall that in some Seyfert nuclei in which variations of the Balmer lines have been reported, the blue and red sides of the line seemed to behave independently: in NGC 7603 (Tohline & Osterbrock 1976), NGC 1566 (quoted by Eggen 1972), and IC 450 (Ulrich 1972; Khachikian & Weedman 1971) for example. This points towards the presence of two main zones, spatially differentiated, which contribute to the Balmer line emission.

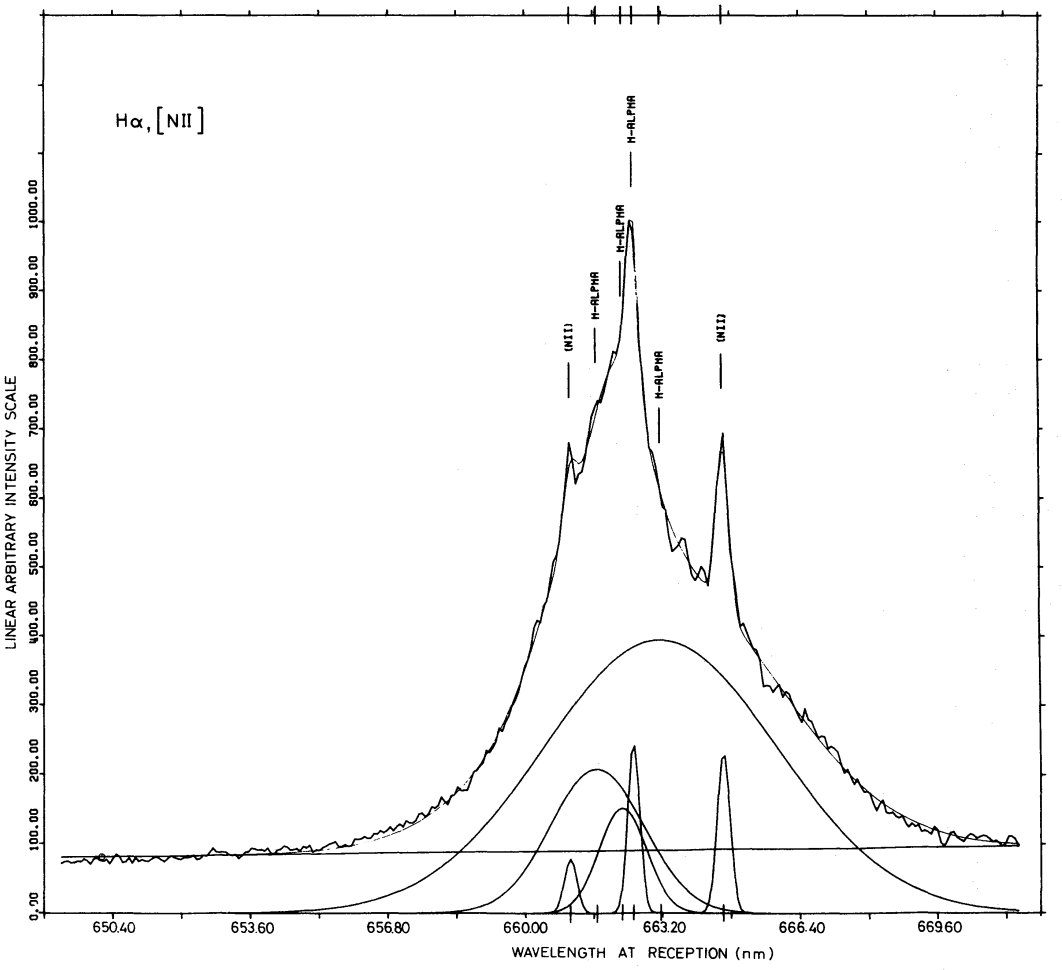

Figure 4. Gaussian analysis of the Hα 656.28 and [N II] 654.81, 658.34 nm lines blend.

4 Discussion

4.1 SYSTEMIC VELOCITY OF NGC 3783

A precise estimate of this quantity is not available, the only interstellar absorption line which might be used is the *K* line which is blended with a galactic *H* line and cannot produce a reliable systemic velocity. Radio H I 21-cm data for NGC 3783 does not yet have the desired precision and no stellar absorption lines are detected in the spectra. Consequently, we have adopted the redshift of the lowest ionization species, z ([O I], [O II], [N II]) = 2930 km s^{-1} to represent the systemic velocity of the galaxy.

4.2 COMPARISON OF THE OBSERVATIONAL PARAMETERS DEFINING THE DIFFERENT LINES OVER THE RANGE O^0 TO Fe^{9+}

Following Ward (1978) we present in Fig. 5 the relationship between the FWHI of the line emitted by a given ion and the corresponding ionization potential χ. In this diagram we have considered only the FWHI of the main contributions ($\geqslant$ 70 per cent of the line) except for [O III] 500.68 nm where two components of about the same weight are present.

Fig. 6 gives the observed relationship between the emission velocity of each component within a line and its FWHI for all the forbidden lines observed in NGC 3783. The error bars

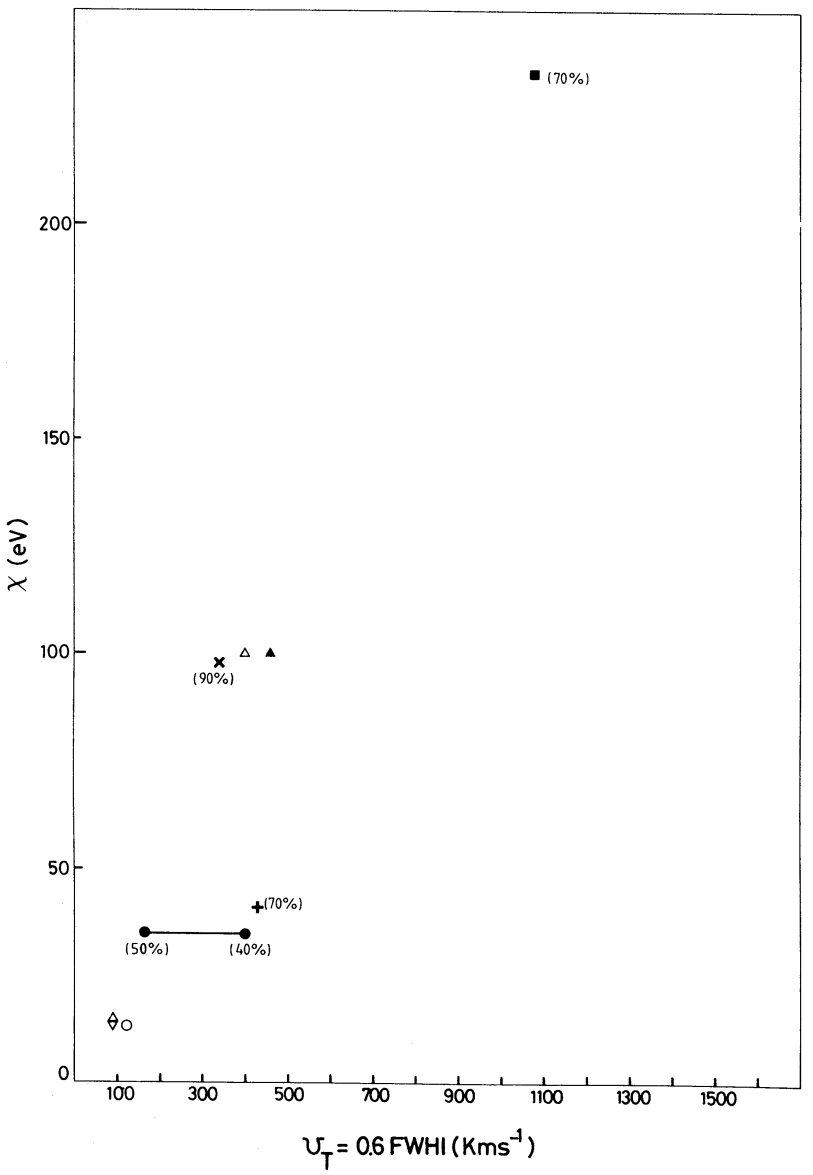

Figure 5. Relationship between the ionization potential (eV) and the turbulent velocity v_T of the component contributing most to each line. The percentage indicates the contribution of this component to the line; if not given, the line was fitted by only one component. Symbols for the points are the following: ●, O^{2+}; ○, O^{+}; ·, O^{0}; ×, Ne^{4+}; +, Ne^{2+}; , N^{+}; ▲, Fe^{6+} 376.03; △, Fe^{6+} 608.69; ■, Fe^{9+}.

provided along the emission velocity axis correspond to the nominal resolution quoted in Table 3. The dependence we find here between these two parameters is quite compatible with previous occasional quotations (Phillips 1976, 1977; Koski 1978; Grandi 1977, 1978; Feldman & Macalpine 1978) reporting systematic blueshifts for forbidden emission lines from highly ionized species in various Seyfert or radio galaxies.

Another way of considering these results is to compare the observed FWHI and blueshifts of the broadest component in each line to the critical density of the corresponding transition (Osterbrock 1974). These relationships are presented in Fig. 7(a) and (b). The point corresponding to the [O I] lines 630.02, 636.39 nm could be omitted since it represents the narrow component of the line, while the broad component, which is in fact relevant for a comparison with the critical density, is suspected to be blended with [S III]

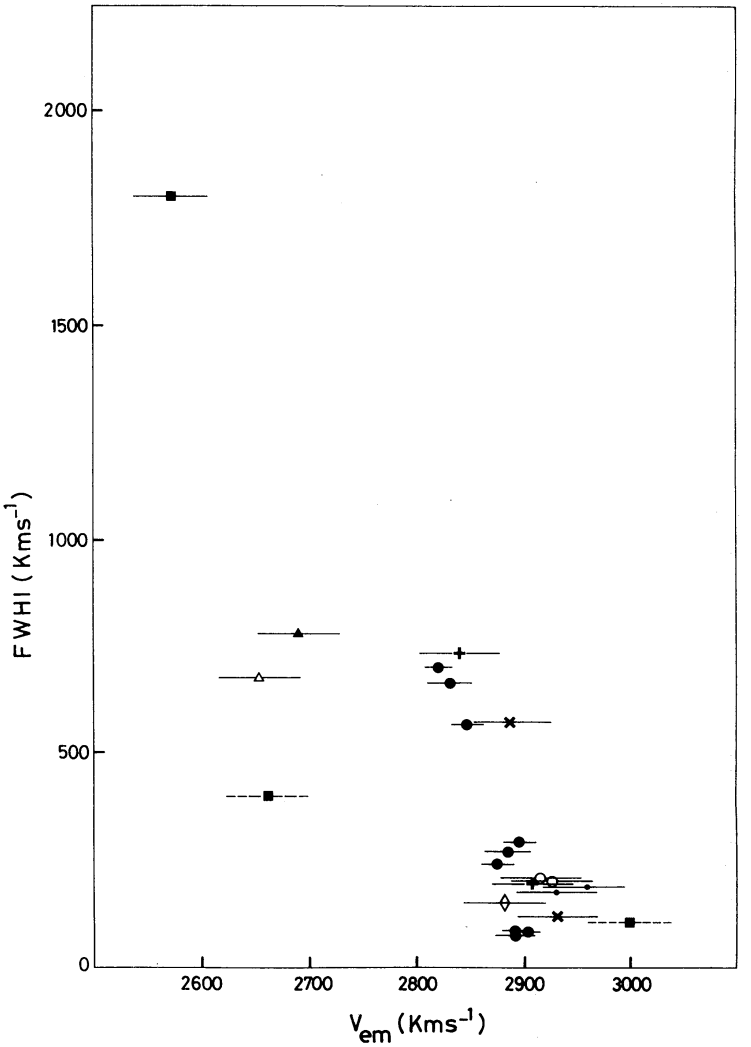

Figure 6. Relationship between the FWHI (km s^{-1}) of each component and its emission heliocentric velocity (km s^{-1}). All the components for each line have been included in that graph and are represented with the same symbols as in Fig. 5. The error bars correspond to the nominal resolution of the data. Dashed error bar means doubtful identification.

(for [O I] 630.03 nm) or with [Fe X] (for [O I] 636.39 nm) and, although this result would be of great importance, cannot easily be measured.

4.3 STRUCTURE OF THE EMITTING ZONES

The previous analysis has established, through the diagrams presented in Figs 5 and 6, that the forbidden lines in this Seyfert nucleus originate in a series of zones characterized by the FWHI and the emission shift of the corresponding emitted lines. Our intention is now to discuss the physical and dynamical state of the gas on the basis of some simple assumptions.

4.3.1. Ionization equilibrium

If we assume that the gas is photo-ionized, the simplest assumption to make is that the source of radiation is point-like and centrally located. The alternative assumption of an

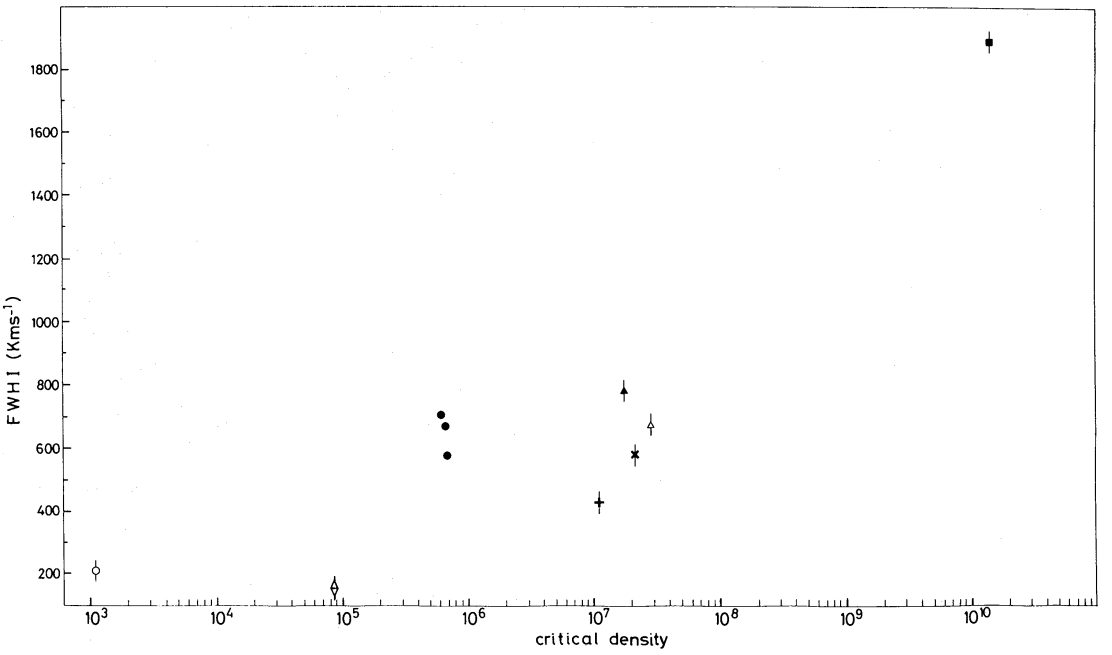

(a)

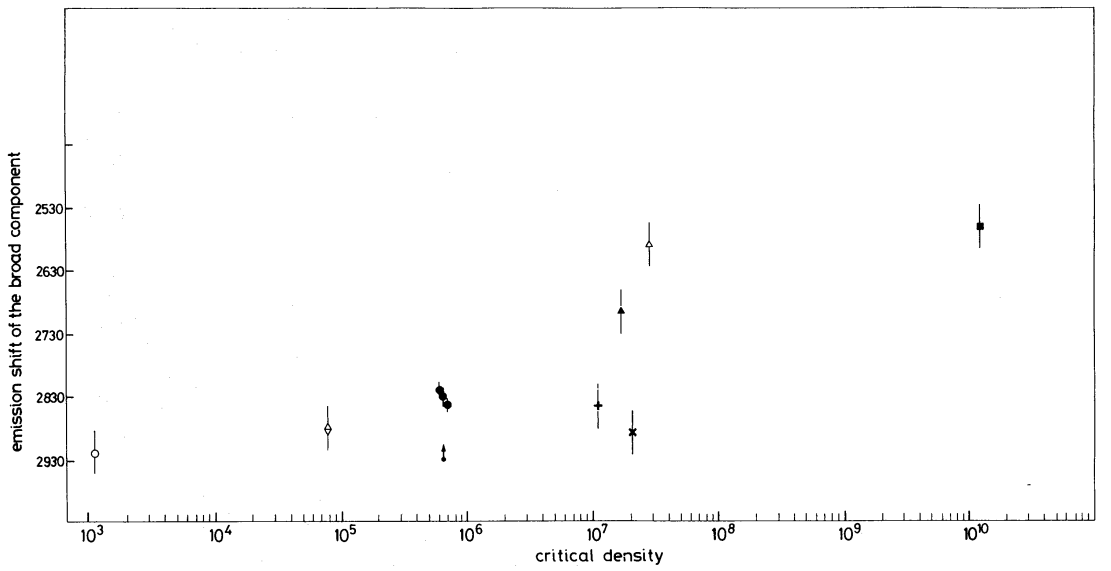

(b)

Figure 7. (a) Relation between the FWHI (km s^{-1}) of the broadest component in each line and the corresponding critical density (cm^{-3}). Same symbols as in Fig. 5. (b) Relation between the observed emission velocity (km s^{-1}) of the broadest component in each line and the corresponding critical density (cm^{-3}). Same symbols as in Fig. 5.

extended source illuminating a disc from outside is inconsistent with the observation that different ions emit different profiles (Shields 1978). Considering the line emission for a particular ion at a distance D from the centre, two conditions must be fulfilled simultaneously:

The presence of this ion;

$N_e \lesssim N_{e,crit}$ in the emitting filaments;

$N_{e,crit}$ being the critical density for the transition considered. A precise model should really be used to discriminate against density distribution effects in the determination of the geometrical configuration. However, under our assumption of a central ionizing source we can derive the minimum distances at which each species has its maximum population, using the equation for ionization equilibrium. From the data given by Ward (1978), the nuclear continuum of NGC 3783 can be represented by a power law

$$L_\nu = 1.01 \times 10^{28} \left(\frac{\nu}{\nu_0}\right)^{-1/2} \text{erg s}^{-1}\,\text{Hz}^{-1},$$

where ν_0 is the frequency at the Lyman limit. The spectral index is determined from optical and infrared data, and we use this to extrapolate into the ultraviolet. For a point situated at a distance D from the UV source, the equation for ionization equilibrium can be written

$$D^2 = \frac{N_i}{N_{i+1} N_e \alpha_{i+1}(T_e)} \frac{1}{4\pi} \int_{\nu_i}^{\infty} \frac{\sigma_{i,\nu} L_\nu \exp(-\tau_\nu)}{h\nu}\, d\nu.$$

For a given species i, this can be solved for the inner and outer boundaries of the zone where i has its maximum fractional population, i.e. between $N_{i-1}/N_i \simeq 1$ and $N_i/N_{i+1} \simeq 1$. For the more highly ionized species, the assumption that $\tau_\nu = 0$ is reasonable, but a proper ionization model should really be used for the lower ionizations. The minimum size is achieved when each line is radiated by gas at its critical density, and the mean distances derived using this assumption are given in Table 5. For the purpose of this approximate calculation we have

Table 5. Characteristic distances for $N_e = N_{e,crit}$ and observational parameters.

Emitted line	$D_{c,min}$ (pc)	$D_{c,max}$ (pc)	$N_{e,crit}$ (cm^{-3})	FWHI ($km\ s^{-1}$)	$v = V - V_{syst}$ ($km\ s^{-1}$)	$\frac{\epsilon(ion)}{\epsilon(O^{2+})}$	$\frac{v_{ff}(ion)}{v_{ff}(O^{2+})}$
[O III] 500.68 nm	39	115	6.5×10^5	670	−100		
[Ne III] 386.87 nm	12	31	1.1×10^7	720	−90	1	1.8
[Ne V] 342.58 nm	1.6	3.5	2.1×10^7	550	−40	50	4.9
[Fe VII] 376.03 nm	1.5	3.1	1.7×10^7	770	−270	10	5.1
608.69 nm	1.2	2.4	2.8×10^7	670	−340	10	5.7
[Fe X] 637.45 nm	1.6×10^{-2}	2.2×10^{-2}	1.2×10^{10}	1800	−400	100	49.0

used hydrogenic recombination coefficients at $T_e = 2 \times 10^4$ K from Spitzer (1978). Photoionization cross-sections were taken from Reilman & Manson (1979). In this table we have added the observed parameters of the innermost slab in each line (largest FWHI and consequently largest emission blueshift) which is expected to have the closest physical conditions to the critical ones.

4.3.2 Dynamical and geometrical considerations

Considering these results on the forbidden and permitted emission lines in NGC 3783, we will try to interpret them within a consistent picture. Each zone is characterized by its distance D to the centre, its density N_e within the emitting filaments, its filling factor ϵ such that $\bar{N}_e = \epsilon N_e$, its mean turbulent velocity and its mean emission shift.

(a) The observed redshift of the main component in the Balmer lines (no. 4) is interpreted in terms of gravitational and Doppler shifts. We consider this component to originate in an accretion disc (AD) rotating around a central massive object. In this frame we can compare the FWHI *and* redshift of the observed component with the corresponding theoretical values predicted by Gerbal & Pelat (1981). Their study includes only

dynamical and kinematical effects, neglecting any radiative transfer considerations; but we know from Ferland *et al.* (1979) that the introduction of these effects diminishes the FWHI, reducing the blue wing. With the kind of standard analysis we perform, using a Gaussian shape for the components, the net result will be a slight underestimation of the real FWHI and a slight overestimation of the redshift, but its seems impossible to escape this difficulty without building a precise model. We derive the following constraints from both the FWHI and redshift of component no. 4 in Hα and Hβ:

inclination of the AD ~ 15°;

distance D of the emitting zone: $D = 10^3 R_S$, where R_S is the Schwarzschild radius. D is then related as follows to the mass of the central object:

$$D = 0.01 \frac{M}{M_8} \text{ pc}, \quad \text{where} \quad M_8 = 10^8 M_\odot.$$

In this zone, N_e is greater than about $10^{10}\,\text{cm}^{-3}$ since none of the forbidden lines shows a component corresponding to the characteristics of this region (FWHI = 3000 km s^{-1}, redshift = 200 km s^{-1}). Moreover, the absence of any detectable redshifted component as well as the range of observed FWHI implies, independently of density effects, that the forbidden lines have to be emitted at distances $D > 10^5 R_S$ in such an AD configuration.

(b) If we now turn to the forbidden line region in which $N_e < 10^{10}\,\text{cm}^{-3}$, two observational facts should be considered:

In NGC 3783, the blueshift increases from low to high ionization species or from small to large electron densities, i.e. from the outermost to the innermost emitting zones.

At the time of writing, published results concerning the emission of shift of forbidden lines from highly ionized species such as [Fe XI] 789.2 nm, [Fe X] 637.45 nm, [O III] 500.68 nm, and [Ne III] 386.87 nm in Seyfert and radio galaxy nuclei, as well as a number of unpublished line profiles in the Seyfert nuclei of NGC 3081, 3516, 4507, 5548, 7469, Mark 1, Mark 3 and 3C 120 (A. Boksenberg 1979 private communication; Briggs *et al.* 1979; R. A. Fosbury & M. Whittle 1980 private communication) all demonstrate, except in one case (Mark 268), the presence of *blueshifts* with respect to low ionization species. Although this sample is not very large (12 objects), we can conclude that generally the forbidden line region is not dominated by a rotational velocity field which should produce redshifts in about 40 per cent of the cases and also FWHI for these lines 10 times larger than observed (Gerbal & Pelat 1981). Alternatively, the observational results can be explained with a radial velocity field characterized by a larger velocity for the higher ionization species. Up to this point, two possible configurations are possible: (i) An ejection of matter plus the presence of some obscuring material in the centre, in order to hide the receding ejecta so that only blueshifts can be detected; although this is an interesting alternative, we shall not discuss it here. (ii) An accretion of matter by the central massive object via the AD, in the form of dense filaments of which only the surface looking towards the central ionizing source is ionized. Each filament must be optically thick to the ionizing radiation as well as to its own radiation, still implying the presence of dust; but ϵ being less than 1, the ionizing radiation can travel large distances.

The hydrodynamic treatment of such a flow is beyond the scope of the present study but is needed to decide whether we are dealing with an outflow or an infall of material.

In fact, both effects might well occur more or less simultaneously on different scales. It would be worthwhile to derive, on theoretical grounds, their order of magnitude and the location of their maximum efficiency. Nevertheless, for the forbidden line region, the likelihood that matter is accreted by a central massive object ($\dot{M} \sim 1\,M_\odot\,\text{yr}^{-1}$ in order to account

Table 6. Summary of the parameters defining the emitting zones in NGC 3783.

Zone	A	B	C	D
Permitted lines★	Hα, Hβ	Hα, Hβ	Hα, Hβ	Hα, Hβ
Forbidden lines★	None	[Fe X]	[Fe VII]; [Ne V], [O III], [Ne III];	[O III], [Ne III]; [N II], [O II]; [O I]
N_e (cm^{-3})	$>10^{10}$	$10^{10}-10^{7}$	10^{7} →	10^{3}
D (pc)	<0.01†	$>0.01-1$	>1 →	$>10^{2}$
FWHI (km s^{-1})	3×10^{3}	2×10^{3}	10^{3} →	$\leqslant 10^{2}$
Emission velocity (km s^{-1})	3200	2500	2600 →	2900/3000
$I(\mathrm{H}\alpha)/I(\mathrm{H}\beta)$‡	3.5	4.2	~2.8	
Dominant velocity field	Rotation AD $i\sim15°$ $10^{3}R_S$	Mixing rotational + radial, outside the AD	Radial, outside the AD	

★ Lines in which a component representing this region is seen.
† Taking $M \leqslant 10^{8}M_{\odot}$ for the central object.
‡ Not corrected for reddening.

for the luminosity of a standard QSO, via this mechanism), led us to consider only the second alternative.

Table 6 summarizes the main regions, together with their parameters, from the discussion or from intercomparison of the results in Table 3. Important parameters for deriving the geometrical configuration precisely are the electron density distribution as well as the filling factors which are both unknown in these zones.

From the results presented in Table 5, we provisionally detail the characteristics of the flow, assuming an infall. Note that in case of an outflow, v being then the escape velocity, the results would be the same.

We assume that the flow of filaments obeys the equation of mass conservation:

$$4\pi D^2 \bar{N}_e v = \text{const},$$

where $\bar{N}_e = \epsilon N_e$. We shall also assume that the observed blueshift $V - V_{syst}$ given in Table 5 roughly represents the infall velocity v. Calibrating this relationship from the values for the broadest component of the [O III] 500.68 nm line, we get the relative filling factor:

$$\frac{\epsilon(\text{ion})}{\epsilon(O^{2+})} \simeq 10^{52}(vD^2N_e)^{-1}\ (\text{CGS}),$$

D^2N_e being given by the ionization equilibrium equation. The results in Table 5 indicate clearly that the coverage of the source by the filaments increases towards the centre.

We also compare the observed v value, regarded as the infall velocity, with the free-fall velocity which depends on $D^{-1/2}$, assuming that the broadest component within each line corresponds to the critical density, and with D taken from Table 5 ($D_{c,\,min}$). Calibrating this free-fall velocity again with respect to the [O III] broad component, we obtain the results presented in Table 5, $v_{ff}(\text{ion})/v_{ff}([\text{O III}])$. They are compatible with the observed $v =$

$V-V_{syst}$ values, except for [Ne v] and [Fe x] which have observed blueshifts too small by a factor of 10.

Apart from the [Ne v] results, which are systematically off the mean relationship, this discussion of both ϵ and infall velocities favours a picture in which the filaments are falling towards the AD and central massive object and are being slowed down possibly by frictional effects. This is also compatible with the observed increase of the FWHI of the lines, then due to the dissipation of kinetic energy into turbulent motions.

5 Concluding remarks

The relationship followed by the components of the various forbidden emission lines, as well as the decomposition of the Balmer Hα and Hβ lines, are consistent with the following picture:

The main redshifted component of the Balmer lines originates in a zone where $N_e > 10^{10}\,cm^{-3}$, dominated by a rotational velocity field, for example an accretion disc, for which we derive an inclination of 15° and a radius of about $10^3 R_S$. This inclination is consistent with the almost face-on aspect of NGC 3783 and may indicate that the rotation axis is constant over a very wide range of spatial scales. Also the consequent lack of rotational broadening may have aided the detection of different linewidths as a function of ionization potential in this galaxy.

The forbidden line emitting zones have $N_e < 10^{10}\,cm^{-3}$ and, from photo-ionization considerations, correspond to distances certainly larger than 10^{-2} pc, and dominated by a radial velocity field which increases towards the centre. In a more speculative way and within the frame of infalling material, we have deduced that the filaments cluster towards the centre and are slowed down via a mechanism which increases macroscopic turbulence. This could explain, at least qualitatively, the increase of the FWHI of the lines emitted in this zone.

To emphasize some consequences of this study:

Observational results of this kind should allow a more detailed analysis of the physical conditions: only line components of about the same dynamical parameters (such as the FWHI), which are expected to come from the same slab of material, should be intercompared to determine T_e or N_e. This appears to be the only hope for making an observational determination of the electron density distribution over the various zones. The same conclusion applies for the electron temperature, but this parameter is not crucial in the determination of the geometrical configuration.

The presence of a transition zone with $N_e \sim 10^5$–$10^6\,cm^{-3}$ which emits the broad component in the [O III] 500.68 nm line, argues in favour of a continuous increase of the electron density in the emitting filaments, towards the centre. This has already been suggested by observation of NGC 1068 and 4151. It is also reminiscent of the $10^6\,cm^{-3}$ N_e value implied by the [O III] 436.32/500.68 nm intensity ratio observed in some radio galaxies (Osterbrock, Koski & Phillips 1976) in which the intermediate zone dominates over regions of lower density.

In all cases where the forbidden lines are important, the Balmer lines have to be cleaned of their contribution from the forbidden line region if it is intended to compare them with theoretical models of the broad line region. Moreover, we think that the actual confusion about Balmer profiles 'with or without red or blue shoulders' comes mostly from this effect. It also appears that forbidden lines from highly ionized species may be emitted close to the central massive object and AD, and might provide some help in understanding these regions because, unlike the Balmer lines, they do not suffer any self-absorption.

Finally, we find weak evidence in NGC 3783 for the presence of a hot diluted gas emitting in the [Fe x] 637.45 nm line.

Acknowledgments

We thank M. Penston, M. Ward and A. Wilson for agreeing to the use of data obtained jointly with R. Fosbury at the AAT. We are gratefully indebted to J. Breysacher and P. Djordano for assistance with the equipment at ESO and to the staff at the CDCA. RAEF acknowledges support from the SRC in the form of an AAT fellowship while some of these observations were made. DP acknowledges the hospitality from ESO during the development of this work.

References

Baranne, A. & Duchesne, M., 1976. *Adv. Electron. electron Phys.*, **40B**, 641.
Bowen, I. S., 1960. *Astrophys. J.*, **132**, 1.
Briggs, S., Boksenberg, A., Carswell, R. F. & Sargent, W. W., 1980. *Mon. Not. R. astr. Soc.*, **191**, 665.
Cooke, B. A., Elvis, M., Maccacaro, T., Ward, M. J., Fosbury, R. A. & Penston, M. V., 1976. *Mon. Not. R. astr. Soc.*, **177**, 121P.
Eggen, O. G., 1972. *Q. Jl R. astr. Soc.*, **13**, 550.
Elvis, M., Maccacaro, T., Wilson, A. S., Ward, M. J., Penston, M. V., Fosbury, R. A. & Perola, G. C., 1978. *Mon. Not. R. astr. Soc.*, **183**, 129.
Feldman, F. F. & Macalpine, G. M., 1978. *Astrophys. J.*, **221**, 486.
Ferland, G. J., Netzer, H. & Shields, G. A., 1979. *Astrophys. J.*, **232**, 382.
Fletcher, R. & Powell, M. J., 1963. *Comput. J.*, **6**, 163.
Gerbal, D. & Pelat, D., 1981. *Astr. Astrophys.*, in press.
Glaspey, J. W., Eilek, J. A., Fahlman, G. G. & Auman, J. R., 1976a. *Astrophys. J.*, **203**, 335.
Glaspey, J. W., Walker, A. H. & Stockton, A., 1976b. *Astrophys. J.*, **210**, 27.
Grandi, S. A., 1977. *Astrophys. J.*, **215**, 446.
Grandi, S. A., 1978. *Astrophys. J.*, **221**, 501.
James, F., 1972. *Function Minimization in Proc. 1972 CERN Computing and Data Processing School*, Pertisau, Austria, CERN 72–21, p. 1.
Khachikian, E.Ye. & Weedman, D. W., 1971. *Astrophys. J.*, **164**, L109.
Koski, A., 1978. *Astrophys. J.*, **223**, 56.
Netzer, H., 1975. *Mon. Not. R. astr. Soc.*, **171**, 395.
Nussbaumer, H. & Osterbrock, D. E., 1970. *Astrophys. J.*, **161**, 811.
Oke, J. B. & Sargent, W. W., 1968. *Astrophys. J.*, **151**, 807.
Osmer, P., Smith, M. & Weedman, D. W., 1974. *Astrophys. J.*, **189**, 187.
Osterbrock, D. E., 1974. *Astrophysics of Gaseous Nebulae*, p. 53, W. H. Freeman and Co., San Francisco.
Osterbrock, D. E., Koski, A. & Phillips, M. M., 1976. *Astrophys. J.*, **206**, 898.
Pelat, D. & Alloin, D., 1980. *Astr. Astrophys.*, **81**, 172.
Pelat, D. & Alloin, D., 1981. *Astr. Astrophys.*, submitted.
Phillips, M. M., 1976. *Astrophys. J.*, **208**, 37.
Phillips, M. M., 1977. *Astrophys. J.*, **215**, 746.
Reilman, R. F. & Manson, S. T., 1979. *Astrophys. J. Suppl. Ser.*, **40**, 815.
Rozelot, J. P., 1970. *Astr. Astrophys.*, **6**, 18.
Shields, G. A., 1978. *Pittsburg Conference on BL Lac objects.*
Spitzer, L. Jr., 1978. *Physical Processes in the Interstellar Medium*, p. 107, J. Wiley and Sons, New York.
Tohline, J. E. & Osterbrock, D. E., 1976. *Astrophys. J.*, **210**, L117.
Ulrich, M. H., 1972. *Astrophys. J.*, **171**, L35.
Ulrich, M. H., 1973. *Astrophys. J.*, **181**, 51.
Walker, M. F., 1968a. *Astrophys. J.*, **151**, 71.
Walker, M. F., 1968b. *Astr. J.*, **73**, 854.
Ward, M. J., 1978. *Ph.D. thesis*, University of Sussex, unpublished.
Wilson, A. S., 1979. *Proc. R. Soc. Lond.*, **A366**, 461.